Biophysical Chemistry 21 (1985) 61–78
Elsevier

BPC 00898

CONSTRUCTION AND PERFORMANCE OF A VARIABLE-FREQUENCY PHASE-MODULATION FLUOROMETER

Joseph R. LAKOWICZ and Badri P. MALIWAL

University of Maryland, School of Medicine, Department of Biological Chemistry, 660 West Redwood Street, Baltimore, MD 21201, U.S.A.

Received 22nd June 1984
Accepted 30th August 1984

Key words: Cross-correlation; Phase modulation; Frequency-domain fluorometry; Fluorescence decay; Kinetics; Rotational correlation time; Time-resolved fluorescence

We describe the construction and performance of a variable-frequency phase-modulation fluorometer. This instrument, which provides modulation frequencies from 1 to 200 MHz, was constructed using commercially available components. To facilitate the introduction of these instruments into other laboratories we describe in detail the chosen components and the principles of operation. The present light source is a continuous-wave helium-cadmium laser, which provides convenient excitation wavelengths of 325 and 442 nm. Modulation of the incident light is provided by one of several electro-optic modulators. The extent of modulation ranges from 1.0 to 0.2 as the frequency increases from 1 to 200 MHz. Phase angles and demodulation factors are measured using the cross-correlation method. The closely spaced frequencies are provided by two direct frequency synthesizers. The phase and modulation measurements are accurate to 0.2° and 0.002, respectively, from 1 to 200 MHz. This accuracy allows considerable resolution of complex decay laws. The usefulness of frequency-domain fluorometry for the resolution of multiexponential decays is illustrated by the analysis of several difficult mixtures. As examples, we resolved a two-component mixture of anthracene (4.1 ns) and 9,10-diphenylanthracene (6.3 ns), and confirmed that the intensity decay of NADH in aqueous buffer is at least a double exponential (0.2 and 0.86 ns). We also resolved an especially difficult mixture of anthracene (4.1 ns) and 9-methylanthracene (4.5 ns), and a three-component mixture with decay times of 1.3, 4.1 and 7.7 ns. Frequency-domain fluorometers appear to be particularly useful for determination of complex decays of fluorescence anisotropy. This capability is illustrated by the determination of rotational correlation times as short as 47 ps for *p*-bis[2-(5-phenyloxazolyl)]benzene (POPOP) in hexane at 40°C, and by the resolution of the two correlation times of anisotropic rotators such as perylene and 9-aminoacridine. Resolution of two anisotropy decay times for 9-aminoacridine is a difficult test because these correlation times differ by less than 2-fold. The resolution of multiexponential decays of intensity and anisotropy possible with this instrument is at least equivalent to that obtained using state-of-the-art time-resolved instruments based on mode-locked laser sources. The ease and rapidity of frequency-domain measurements, the relative simplicity of the equipment, the accuracy of the measurements and the lack of significant systematic errors indicate that frequency-domain fluorometry will be widely useful in chemical and biochemical research.

1. Introduction

Fluorescence spectroscopy is widely used in biochemical research because of its high inherent sensitivity and the time scale of the phenomenon [1,2]. Fluorescence emission typically occurs within nanoseconds of light absorption, which is also the time scale of dynamic processes in biochemical samples such as rotational diffusion of proteins and membrane-bound fluorophores, spectral relaxation of biopolymer-bound fluorophores and diffusion of quenchers over distances of 10–50 Å. Because of the complexity of biological macromolecules it is often necessary to resolve multiexponential decays of fluorescence intensity or anisotropy. For example, the decay times of fluoro-

Abbreviation: POPOP, *p*-bis[2-(5-phenyloxazolyl)]benzene.

phores are sensitive to their local environment and biological macromolecules often contain fluorophores in several distinct locations. It is of interest to resolve the emitting species, which is accomplished by resolution of the decay law of the fluorescence emission. Similarly, the rotational diffusion of macromolecule-bound fluorophores depends upon the size, shape and rigidity of the rotating unit. These dynamic properties of the macromolecule can be revealed by the time-resolved decays of fluorescence anisotropy.

Determination of the time-resolved decays of intensity or anisotropy can, in principle, be accomplished using measurements in either the time domain or the frequency domain. In the time domain one measures the time-dependent response of the sample following pulsed excitation. In the frequency domain one measures the phase angle and modulation of the emission relative to the intensity-modulated incident light. During the past 15 years there has been considerable progress and emphasis on time-domain measurements. This is because of the sensitivity and accuracy of time-correlated single-photon counting [3,4], continued advances in time resolution and precision resulting from the use of mode-locked and cavity-dumped laser light sources [5–9], and because of the use of microchannel plate photomultiplier tubes with subnanosecond response times. These recent instruments are now capable of resolving closely spaced fluorescence lifetimes [6,7].

Phase-modulation fluorometers were constructed prior to the development of time-domain instruments [10–14]. It is generally recognized that these instruments are especially useful for measurement of subnanosecond lifetimes. However, most phase-modulation fluorometers operate at only one to three fixed modulation frequencies. Even with very precise data, the limited number of frequencies does not allow the resolution of complex decays of intensity or anisotropy. We note that some successful resolutions have been accomplished [15–17], but that phase-modulation fluorometry has not been generally useful for resolution of complex decay laws. Recently, several laboratories described phase-modulation fluorometers capable of operation at continuously variable frequencies [18–20]. However, only the instrument of Gratton and Limkeman [18] has been demonstrated to be capable of resolving mixtures of fluorophores [21], resolving multiexponential decays of fluorescence anisotropy [22], and of determining time-resolved emission spectra [23,24].

In this report we describe the construction and performance of a similar instrument. We found that such instruments can be constructed quite easily using commercially available components. Assembly of the instrument required less than 1 month. Only a minor amount of specialized circuitry is required. To facilitate the availability of these instruments we describe in some detail the components required, and our reasons for selecting these particular devices. Hopefully, these details will be valuable to other laboratories who may wish to construct a frequency-domain fluorometer. We also present data which illustrate the considerable resolving power of this instrument. In particular, we describe the resolution of closely spaced two- and three-component decays of intensity, and the resolution of two-component decays of anisotropy.

An essential component of the frequency-domain measurements is the ability to use the phase and modulation data to recover the time-domain parameters. We use the procedure of nonlinear least squares [25,26]. In principle, such techniques are straightforward. In practice, their implementation requires considerable effort. Software is presently available to analyze multiexponential decays of intensity and anisotropy, and to determine time-resolved emission spectra. Our programs are in BASIC, run under either RT-11 or the MINC operating system. To eliminate the need of other researchers to duplicate our efforts these programs are available from J.R.L. upon request.

2. Description of the phase-modulation fluorometer

A schematic description of our instrument is shown in fig. 1. Briefly, the overall operation is as follows. The output of the CW-laser is intensity modulated in an approximately sinusoidal manner at a frequency F. The intensity-modulated light is used to excite the sample, and the emission is observed using a photomultiplier. Another photo-

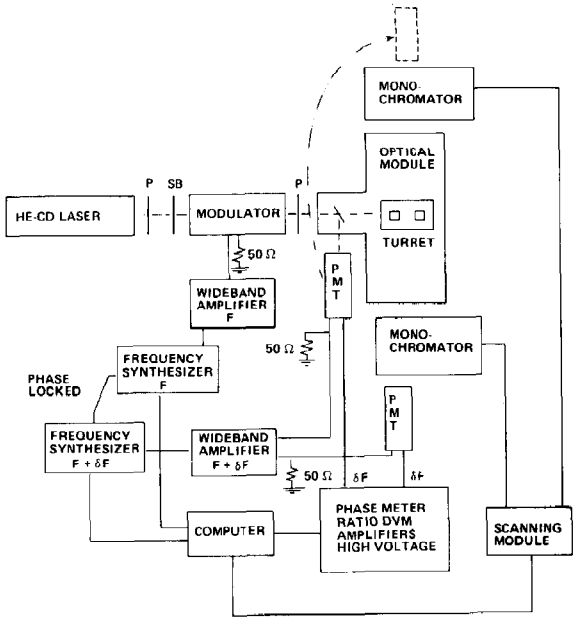

Fig. 1. Schematic representation of the variable-frequency phase-modulation fluorometer. P, polarizer; SB, Soleil-Babinet compensator; F, frequency; δF, cross-correlation frequency; PMT, photomultiplier tube.

multiplier tube (PMT) is placed near a quartz beam splitter and is used as a phase reference. This PMT can also be positioned in the T-format location for differential polarized phase measurements. Measurement of the phase angle difference between the sample and reference emission is accomplished by rotation of a turret. The phase angle difference (ϕ_ω) and the relative modulation of the sample (m_ω) can be measured relative to either scattered light or a reference fluorophore [27]. The subscript ω refers to the modulation frequency, expressed in rad/s ($\omega = 2\pi F$). Detection of the emission is performed using the cross-correlation method [14,18]. Specifically, the gain of the PMTs is modulated at the frequency $F + 25$ Hz, where F is the modulation frequency of the incident light. The phase and modulation are measured at the 25 Hz cross-correlation frequency by a time-interval counter and a ratio digital voltmeter, respectively. The two closely spaced frequencies are provided by two frequency synthesizers which are each driven by the same crystal reference source (phase-locked). The data are averaged and stored by an interfaced Apple IIe computer. Measurement at 20 modulation frequencies typically requires 1 h for data acquisition. In the following sections we describe the individual components, and our reasons for selecting these components (table 1).

2.1. Laser light source

A laser is needed for the light source not because of its coherence, but because of the small aperture of most electro-optic modulators. These devices are typically 3–20 cm long, with optical apertures of about 2 mm. Furthermore, the light must be highly collimated for significant modulation. Consequently, only laser sources are practical for reasonable throughput of light intensity. This is an unfortunate limitation because the excitation of many biochemical samples requires ultraviolet light and ultraviolet lasers are less powerful and more expensive than visible lasers or arc lamps. We have not tried to modulate the output of an arc lamp. This may be possible at lower frequencies. We chose an He-Cd laser because of its output at 325 nm. This wavelength is generally useful for excitation of many probes, but unfortunately this line cannot be used to excite tryptophan fluorescence from proteins. The argon-ion laser is another useful source which can provide continuous output at 351 nm. This laser can also be mode-locked and cavity-dumped, which could be valuable if it becomes possible to use the harmonic content of a laser pulser train, as described by Gratton and Lopez-Delgado [28]. Also, argon lasers can provide considerably higher power than can the He-Cd lasers. This alternative source should be considered if a frequency-domain instrument is to be constructed.

2.2. Modulator and light path

Intensity modulation of the laser light is accomplished using an electro-optic modulator. In response to an applied electric field these devices change linearly polarized light into circularly polarized light. The theory and operation of these devices have been described previously [29–31].

Table 1

Components of the variable-frequency phase-modulation fluorometer

Component	Approximate cost ($) (1983)
Light source	
Helium-cadmium laser, Liconix, model 4240B, 10 mW at 325 nm, 40 mW at 442 nm	11000
Modulators	
(1) Transverse field electro-optic modulator, Lasermetrics, LMA-1, KD * P	900 [a]
(2) Longitudinal field electro-optic modulator, Interactive Radiation, model 102-020	700
(3) Longitudinal field electro-optic modulator, Interactive Radiation, model 101-020	500 [a]
(4) Longitudinal field electro-optic modulator, Lasermetrics 1042, 10 mm aperture	2100 [a]
Optical path	
Soleil-Babinet compensator, Special Optics	1700
Broadband polarization rotator, Special Optics model 8-9010-$\frac{1}{2}$	550 [a]
Laser polarizers, Special Optics, M7-1212, 10 mm with broadband anti-reflection coating (270-600), two needed, $545 each	1090
Electronics (radiofrequency)	
Frequency synthesizers, Program Test Sources, PTS-500M, two needed, 1–500 MHz	16000 [b]
r.f. power amplifier for modulator, EN1 model 525L, 25 W, 1–500 MHz	4400 [c]
r.f. power amplifier for cross-correlation detection at the photomultiplier, ENI 601L, 1 W, 0.1–1000 MHz	1400
r.f. attenuators, Wavetek/Indiana, models 5080 and 5110	600 [a]
r.f. coaxial load resistors, Bird electronics models 8164 (100 W) and 80 M (5 W)	300
Two-way power dividers, Anzac model T-1000	95
Directional r.f. power meter and crystals, Bird Electronics, model 4410	600
Directional r.f. power meter, Bird Electronics, model 4304	325
Electronics (general)	
d.c. and a.c. (25 Hz) signal amplifier, high-voltage supplies for PMTs, phase meter and ratio DVM, with an SLM Instruments, model 4800 mainframe, minus the three-frequency electronics	13400
Interface package and software for an Apple IIe	2990 [a]
Optical components	
Optical module, SLM model OP-450	3500
PMT housings and Hamamatsu 928 PMTs, SLM	2900
Two-position turret	1150
Motorized monochromator (ML 320) and controller (SML 2100), SLM	7600 [a]
Miscellaneous components	
Optical table, 4×10 feet (71-177) with vibration isolation supports (62-125), Technical Manufacturing Co.	4700 [a]
He-Ne laser, 0.5 mW, Spectra Physics, useful for alignment of optics	340 [a]
Calibrated rotary mounts for polarizers, 60-1025-A100, Special Optics	200 [a]
Oscilloscope, Hewlett Packard 1725 A, 275 MHz, dual trace	4500 [a]

[a] A functional instrument can be constructed without these items.

[b] Two frequency synthesizers, each capable of frequencies to 160 MHz, can be purchased for about $12000.

[c] A 25 W amplifier to 160 MHz (530 L) can be purchased for about $1500.

The electro-optic modulator is placed between crossed polarizers (fig. 2). We use a Soleil-Babinet compensator (SB) to provide an optical bias. An advantage of the SB compensator is that any degree of bias can be obtained at any wavelength. This is functionally equivalent to the voltage bias shown in fig. 3.

An important characteristic of an electro-optic

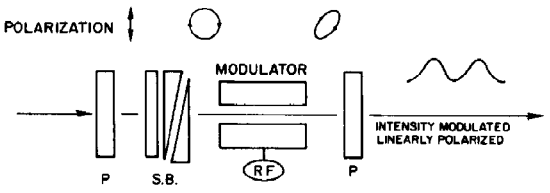

Fig. 2. Optical arrangement for an electro-optic modulator. P, polarizer; SB, Soleil-Babinet compensator; RF, radiofrequency signal.

modulator is the voltage required to rotate the polarization by $\lambda/4$ or $\lambda/2$, referred to as the quarter-wave or half-wave voltages, respectively. The lowest possible value of the half-wave voltage ($V_{\lambda/2}$) is preferred because it is difficult to generate high-voltage signals at high frequencies. Electro-optic modulators are available in which the electric field is either transverse or parallel (longitudinal) to the light path. Transverse field modulators have lower values of $V_{\lambda/2}$, but they also have larger capacitance, which may limit the frequency response. Longitudinal field modulators are available with low capacitance, but larger values of $V_{\lambda/2}$. The highest modulation frequency obtainable with an electro-optic modulator depends not only on the capacitance, but also on the particular design. We tested several modulators in addition to those listed in table 1. Frequently, the modulation became increasingly unstable at higher frequencies. This was apparently due to the absorption of radiofrequency (r.f.) power and subsequent temperature gradients within the modulator. It is known that small temperature gradients can result in variation in the extent of modulation [29]. The extent of r.f. power absorption probably depends upon the materials used for the electrodes, and the contact between the electrodes and the crystals.

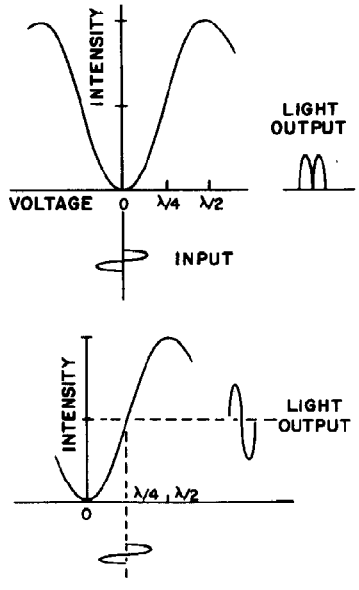

Fig. 3. Modulated intensity from an electro-optic modulator. The upper drawing shows the modulated intensity without an electrical or optical bias, the lower drawing includes a $\lambda/4$ bias. Redrawn from ref. 32.

Fig. 3 illustrates two possible modes of using an electro-optic modulator. If an r.f. voltage is applied to the modulator, and no optical or electrical bias is applied, then the transmitted light is modulated at twice the applied frequency (fig. 3, top). We have not used this doubling procedure because we consistently obtained higher modulation and a larger frequency range with the nondoubling mode (below). This may have been a result of the high half-wave voltage of our modulators, which made it difficult to obtain adequate modulation in this doubling mode with reasonable amounts of r.f. power (25 W).

We use the modulators in the approximate linear mode (fig. 3, bottom). This can be accomplished using either a voltage bias or an optical bias. We chose to use an optical bias provided by a Soleil-Babinet compensator, which is continuously and accurately adjustable. Also, because a constant d.c. voltage is not applied to the modulator, there is a reduced danger of electrolysis at the electrodes. The incident light from the laser is linearly polarized, but we found it convenient to use another polarizer prior to the compensator (fig. 2). The modulator is placed between crossed polarizers. The light is transformed into elliptically polarized light by the SB compensator (fig. 2). If the SB compensator is adjusted to the $\lambda/4$ position then the light incident on the modulator is circularly polarized. When a voltage is applied the polarization is rotated further. Hence, the transmission is varied, and the incident light is mod-

ulated at the applied frequency. If the applied voltage is small then the modulation can be highly linear. Most technical descriptions of electro-optic modulators suggest biasing the transmission at the quarter-wave point ($\lambda/4$) using a quarter-wave plate. In practice, we could not obtain adequate modulation using this degree of bias. This is because the practically available voltages (a maximum 100 V peak-to-peak for 25 W into 50 Ω) did not provide more than $\lambda/10$ rotation. The degree of modulation can be increased by decreasing the bias to between $\lambda/5$ and $\lambda/20$. This is easily accomplished using the SB compensator. However, the increased modulation is achieved at the expense of a decreased total intensity. Adjustment of the bias towards zero results in increased harmonic content in the modulated light. However, we found that this did not cause any systematic errors. Apparently, the harmonics are eliminated by cross-correlation detection [18].

We successfully used four different electro-optic modulators. The Lasermetrics LMA-1 transverse field modulator is very convenient because of its low half-wave voltage (480 V at 325 nm). This allows a larger bias and hence greater light intensity than with the longitudinal field modulators (Inrad 101-020, Inrad 102-020 and Lasermetric 1042). However, the LMA-1 appeared to absorb r.f. power above 140 MHz, resulting in unstable modulation and rapid failure. Below 140 MHz it was reliable and stable. However, it was necessary to keep the r.f. power low (< 7 W), otherwise the extent of modulation was not stable. The 102-020 102-010 and 1042 all provided modulation to 220 MHz, but typically with less intensity than the LMA-1. This is because of their high half-wave voltages, which required that the SB compensator be adjusted closer to the zero-wave position. The half-wave voltage of the 102-020 and 1042 is 900 V at 325 nm, and that of the 101-020 is 1800 V at 325 nm. The Inrad 102-020 and Lasermetrics 1042 each contain two crystals, which decreases $V_{\lambda/2}$ by 50% relative to the 101-020. We were surprised that useful modulation and intensity could be obtained using the single crystal modulator from Interactive Radiation (101-020). Previously it was thought that the high half-wave voltage of such a device (1800 V at 325 nm) would prevent the attainment of adequate modulation [33]. However, useful modulation was obtained at the expense of intensity, i.e., by decreasing the optical bias of the compensator towards zero. The LMA-1 and 1042 were easier to align than the 102-020 and the 101-020, which were quite sensitive to orientation. The extent of modulation was typically near 1.0 at 1–10 MHz, near 0.5 from 10 to 100 MHz, and decreased gradually to 0.2 at 200 MHz.

In our judgement, power absorption by a modulator can be recognized by an increase in the intensity of the unmodulated light and by unstable modulation. The excess intensity appears to be dependent upon r.f. power and frequency, and varies with a time over a period of seconds. In daily operation we avoid power levels or frequencies at which the modulation is unstable, which we believe is due to power absorption. It is known that temperature gradients induce birefringence changes in electro-optic modulators [29]. At present it appears that the best overall performance is provided by the Lasermetrics 1042. It provides the highest overall modulation at frequencies to 230 MHz, where the modulation can be as high as 0.10. This modulator appears to provide the most stable modulation, which may be a consequence of the larger size of the crystals. We found that the Lasermetrics 1042 and both Inrad modulators radiated r.f. power into the room, which is evident by an increase in the d.c. component of the signal as the r.f. power applied to the modulator is increased. Apparently, the radiated r.f. is detected by the PMTs and/or amplifiers, and this appears as unmodulated signal. This problem was especially pronounced at frequencies near 200 MHz. Fortunately, a simple solution was available. We constructed cylindrical copper enclosures for these modulators which shielded both the modulator body and the electrical leads. The thickness of the enclosure was about 1 cm. The r.f. power was applied to the modulator using a BNC bulkhead connector positioned on the enclosure.

Other modulators were evaluated for use with our instrument. The traveling-wave modulators appeared promising because of bandwidths extending to 1 GHz. Unfortunately, the TWAM-20 modulator from Quantum Technology with a specified bandwidth of 1 GHz was found to be

completely unsuitable, apparently due to excess thermal sensitivity.

2.3. Frequency synthesizers

The use of cross-correlation detection requires that two frequencies be available (F and $F + \delta F$), and that frequency difference (δF) be precise and stable. We chose $\delta F = 25$ Hz since this is the cross-correlation frequency used in the electronics package available from SLM Instruments (model 4800). The cross-correlation frequency must be accurate over the entire frequency range of the measurements. Hence, it is necessary to generate the required frequencies to an accuracy of 1 Hz or better. These requirements are satisfied for a reasonable cost by the synthesizers from Program Test Sources. Their frequency range is 1–500 MHz, adjustable to ± 0.1 Hz. To improve relative stability the two synthesizers are phase-locked.

2.4. Radiofrequency amplifiers

The electro-optic modulators require the highest reasonable voltage (to about ± 500 V) over a wide frequency range. We chose the ENI 525L as a compromise of cost and frequency range. It provides 25 W, which yields a maximum peak-to-peak voltage (V_{pp}) of about 100 V ($V_{pp} = 2.8 \times$ (power $\times$ resistance)$^{1/2}$). We often remove the 50 Ω termination resistor at the modulator (fig. 1), which can increase V_{pp} by 2-fold. However, the r.f. power is then reflected back towards the amplifier, and standing waves can complicate the frequency response. An advantage of the ENI amplifier is that it is fully protected against reflected power. Hence, one can obtain the increased modulation without damage caused by the reflected power from the unterminated transmission line. The cable length between the amplifier and the modulator must be 30 cm or less to minimize standing-wave reflections.

Relatively little voltage is required to modulate the phototube gain. We use a 1 W amplifier (EN1 601L). The output was shared by a two-way power divided, and each side terminated by 50 Ω at dynode 9 of the PMTs [18]. We used the dynode chain provided by SLM, and simply disconnected their tuned circuits and connected the divided r.f. output (see section 2.7). Typically we used 2 V peak-to-peak to modulate the PMT gain. The apparent modulation and instrument performance were rather independent of this voltage level.

2.5. Main electronics

The model 4800 electronics rack from SLM Instruments provides a convenient grouping of needed components. This component is a portion of their three-frequency phase fluorometer. The three-frequency r.f. amplifiers are not needed, nor is the phase shifter. The rack contains the needed high-voltage supplies, d.c. and a.c. (25 Hz) amplifiers, a time-interval counter (phase meter) and a ratio digital voltmeter (DVM). Conveniently, this module can be purchased with hardware and software for an interface to an Apple IIe. We found it convenient to use this interface and software for input of the phase and modulation values to the computer. However, the analysis sections of the software are not useful for the frequency-domain measurements.

In the SLM 4800 the a.c. gain is fixed and coupled with the d.c. gain. This is inconvenient because it is often desirable to increase the a.c. gain to compensate for low modulation values. We inserted an additional stage of variable a.c. gain (1–100-fold). A detailed description of this circuit is available upon request. Also, we modified the inputs to the DVM so that any of the four signals could be transmitted into either of the two DVM inputs. This is necessary for measurement of the ratio of the polarized modulated amplitudes (Λ_ω), which is the ratio of the a.c. values observed for vertically and horizontally polarized emission. This ratio is used in the determination of time-resolved anisotropies. To eliminate drifts in Λ_ω due to changes in the degree of modulation, each a.c. intensity is measured as the ratio of its actual value divided by the a.c. intensity measured by the reference PMT. This PMT can be located either at the beam splitter or at the T-format position (fig. 1).

2.6. Optical components

The optical module from SLM (OP-450) provides a convenient sample compartment with built-in mounts for optical filters and polarizers, and the possibility of T-format measurements. The turret from the SLM phase fluorometer is also useful for the variable-frequency measurements.

The Hamamatsu R928 phototube appears to be a good choice. To date we have not noticed any substantial color effect, in agreement with time-resolved measurements [34]. It has good sensitivity, extending to 800 nm, and it is easily modulated at the last dynode. At present we do not know if the PMT is the reason for the low apparent modulation values above 200 MHz. From the 2.2 ns rise time of this PMT one predicts a decrease in the apparent modulation to 2-fold less than the actual value at 75–180 MHz [30,35]. If necessary, it may be possible to increase the time response of this PMT by focusing the image on the photocathode and careful optimization of the dynode chain [36,37]. However, our initial attempts using modified dynode chains did not yield the improvements expected from refs. 36 and 37. If measurements considerably above 200 MHz are required then it seems desirable to consider other photomultiplier tubes. For instance, we did obtain a slightly improved frequency range using a Amperex 56 DUVP, which is a focused PMT with a 2 ns rise time. However, the R928 provides completely satisfactory performance to 200 MHz.

2.7. Dynode chain

We use a simple modification of the dynode chain from SLM Instruments. In this circuit the photocathode and dynodes 1–8 are each separated by 470 kΩ resistors and 5000 pF capacitors. A 1 MΩ trim potentiometer separates dynode 8 and ground, and the modulation dynode [9] is biased near 0.1 V using the potentiometer. We tried other arrangements, but this simple circuit was found to give the best overall performance. It is important to recognize that the apparent modulation may depend upon the overall voltage on the photomultiplier tube. This dependence is especially evident at low voltages (< 500 V) and higher frequencies (> 100 MHz). (The actual voltage on the Hamamatsu R928 is about one-half of the applied voltage due to a voltage divider in the PMT housing). Apparently, at low voltages the time or frequency response of the PMT is less than at higher voltages.

To improve the frequency response of the PMTs we tried to modify the dynode chain in two ways. First, we placed a 150 V zener diode from the photocathode (PC) to the first dynode (D1). We reasoned that this would improve the frequency response because the of transit time differences from PC to D1. Unfortunately, the presence of the diode decreased the apparent modulation at high frequencies with low voltage, but had no effect at high voltage or low frequency. Apparently, the transient time spread through the dynode chain limits the frequency response, and not the transit time from PC to D1. When the diode is inserted, and the overall voltage kept constant, there is a smaller potential drop between each dynode. This results in decreased high-frequency response.

We also tried the circuit described by Gratton and Limkeman [18] in which D9 is biased at a constant voltage near the center of the characteristic gain curve. An advantage of this circuit is that the PMT gain modulation may be more linear, and the D9 bias should be independent of overall voltage. To date we found no clear advantage of this circuit over the trim potentiometer from D8 to ground with a bias near 0.1 V.

2.8. Miscellaneous components

Radiofrequency attenuators are essential for adjusting the output of the frequency synthesizers prior to input to the r.f. amplifiers. r.f. power meters are needed to measure the output of the amplifiers. The Model 4410 provides accurate measurements over a wide range of frequencies and power levels. A convenient feature of the model 4304 is that it has an attenuated r.f. output which may be used to view the r.f. waveforms. An inconvenient feature of this power meter is that it does not allow power reading below 25 MHz.

An oscilloscope is essential for examining the r.f. signals incident upon the PMTs and the modulators. As the frequency is varied it is necessary to

adjust the r.f. power levels to remain within the nonsaturated range of the amplifiers. We chose the Hewlett Packard 1725A. This dual-trace scope allows observation of both r.f. signals, and its bandwidth of 275 MHz is adequate to cover the available modulation frequencies.

3. Theory

3.1. Decays of fluorescence intensity

The variable-frequency phase (ϕ_ω) and modulation (m_ω) data were analyzed using the nonlinear least-squares method [25,26]. This procedure is described in detail in other reports [21,25]. Briefly, the expected values at each modulation frequency ($\phi_{c\omega}$ and $m_{c\omega}$) can be predicted for an assumed impulse-response function. For a mixture of n fluorophores, each of which displays a single lifetime, the impulse function ($I(t)$) is a sum of exponential decays

$$I(t) = \sum_i^n \alpha_i e^{-t/\tau_i}. \tag{1}$$

In this expression τ_i is the decay time of the i-th component and α_i the preexponential factor of this component. The fractional contribution of each component to the steady-state intensity is given by

$$f_i = \frac{\alpha_i \tau_i}{\sum_i \alpha_i \tau_i} \tag{2}$$

At each modulation frequency expected values of $\phi_\omega (= \phi_{c\omega})$ and $m_\omega (= m_{c\omega})$ are given by [38,39]

$$\phi_{c\omega} = \arctan(N_\omega / D_\omega) \tag{3}$$

$$m_{c\omega} = (N_\omega^2 + D_\omega^2)^{1/2} \tag{4}$$

where $\omega = 2\pi \times$ frequency (in Hz), and

$$N_\omega J = \sum_i \frac{\alpha_i \omega \tau_i^2}{1 + \omega^2 \tau_i^2} \tag{5}$$

$$D_\omega J = \sum_i \frac{\alpha_i \tau_i}{1 + \omega^2 \tau_i^2} \tag{6}$$

and

$$J = \sum_i \alpha_i \tau_i. \tag{7}$$

The goodness of fit between the measured values and an assumed model is judged by the value of χ^2, which is given by

$$\chi^2 = \sum_\omega \frac{1}{\sigma_{\phi\omega}^2} (\phi_\omega - \phi_{c\omega})^2 + \sum_\omega \frac{1}{\sigma_{m\omega}^2} (m_\omega - m_{c\omega})^2 \tag{8}$$

In this expression ϕ_ω and m_ω refer to the measured phase and modulation values at the indicated frequency, respectively. $\sigma_{\phi\omega}$ and $\sigma_{m\omega}$ are the errors of the measured phase and modulation values under the chosen experimental conditions.

A more familiar measure of the goodness-of-fit is the value of reduced χ^2,

$$\chi_R^2 = \frac{\chi^2}{\nu} = \frac{\chi^2}{2Nq - p} \tag{9}$$

where the number of degrees of freedom is given by $\nu = 2Nq - p$. N is the number of modulation frequencies, q the number of samples and p the number of floating parameters. Except for the Global analysis (below) the number of samples is always one. If the assumed model is appropriate for the sample, and if the errors are random and properly estimated by $\sigma_{\phi\omega}$ and $\sigma_{m\omega}$, then χ_R^2 is expected to be near unity.

3.2. Global analysis of closely spaced decay times

The ability to resolve closely spaced lifetimes can be increased by measuring the phase and modulation values for several samples (s) in which the relative concentrations of the components is varied. In the fitting procedure the values of τ_i are restricted to be independent of sample (s) but the $\alpha_i(s)$ values are dependent upon the sample. The value of χ^2 is given by

$$\chi^2 = \sum_s \sum_\omega \frac{1}{\sigma_{\phi\omega}^2} (\phi_\omega(s)_{c\omega} - \phi_{c\omega}(s))^2 + \sum_s \sum_\omega \frac{1}{\sigma_{m\omega}^2} (m_\omega(s) - m_{c\omega}(s))^2 \tag{10}$$

In this expression we assume that the random errors in ϕ_ω and m_ω are not dependent upon the particular sample.

3.3. Decays of fluorescence anisotropy

Time-resolved anisotropies can be determined from the phase difference (Δ_ω) between the perpendicular ($\phi_\perp$) and parallel ($\phi_\parallel$) component of the modulated emission ($\Delta_\omega = \phi_\perp - \phi_\parallel$) and the amplitude ratio (Λ_ω) of the parallel ($m_\parallel$) and the perpendicular ($m_\perp$) components of the modulated emission ($\Lambda = m_\parallel / m_\perp$). These values were measured using the T-format method [2,17]. The decays of the parallel ($\parallel$) and perpendicular ($\perp$) components of the emission are given by

$$I_\parallel(t) \text{-} \tfrac{1}{3} I(t)(1 + 2r(t)) \tag{11}$$

$$I_\perp(t) \text{-} \tfrac{1}{3} I(t)(1 - 2r(t)) \tag{12}$$

where $r(t)$ is the time-resolved decay of anisotropy. Generally, $r(t)$ can be described as a multiexponential decay,

$$r(t) = r_0 \sum_i g_i e^{-t/\theta_i} \tag{13}$$

where r_0 is the limiting anisotropy int he absence of rotational diffusion. The expected values of Δ_ω ($\Delta_{c\omega}$) and Λ_ω ($\Lambda_{c\omega}$) can be calculated from the sine and cosine transforms of the individual polarized decays [2,38],

$$N_i = \int_0^\infty I_i(t) \sin \omega t \, dt \tag{14}$$

$$D_i = \int_0^\infty I_i(t) \cos \omega t \, dt \tag{15}$$

The frequency-dependent values of Δ_ω and Λ_ω are given by

$$\Delta_{c\omega} = \arctan\left(\frac{D_\parallel N_\perp - D_\perp N_\parallel}{N_\parallel N_\perp + D_\parallel D_\perp} \right) \tag{16}$$

$$\Lambda_{c\omega} = \left(\frac{N_\parallel^2 + D_\parallel^2}{N_\perp^2 + D_\perp^2} \right)^{1/2} \tag{17}$$

where the N_i and D_i are calculated at each frequency. The parameters describing the anisotropy decay are obtained by minimizing the squared deviations between measured and calculated values,

$$\chi^2 = \sum_\omega \frac{1}{\sigma_{\Delta\omega}^2} (\Delta_\omega - \Delta_{c\omega})^2 + \sum_\omega \frac{1}{\sigma_{\Lambda\omega}^2} (\Lambda_\omega - \Lambda_{c\omega})^2 \tag{18}$$

In this expression $\sigma_{\Delta\omega}$ and $\sigma_{\Lambda\omega}$ are the estimated experimental uncertainties in the measured quantities (Δ_ω and Λ_ω).

In this report we used two models to describe the decays of anisotropy. For an isotropic rotator we used

$$r(t) = r_0 e^{-t/\theta}. \tag{19}$$

For the anisotropic rotator model we used an anisotropy decay law with two correlation times,

$$r(t) = r_0 \left(g_1 e^{-t/\theta_1} + g_2 e^{-t/\theta_2} \right) \tag{20}$$

with $g_1 + g_2 = 1$, g_1 as a floating parameter and r_0 fixed. In some cases the floating parameters were $r_0 g_1$ and $r_0 g_2$. More details are given in refs. 22 and 23.

4. Results and discussion

4.1. Single exponential decays

To illustrate the ability of this instrument to measure short fluorescence lifetimes we chose to present data for fluorescein in water (4.3 ns) and for rose bengal in ethanol (0.83 ns) and in water (0.13 ns). Frequency-dependent values of the phase angle and modulation for these single-component solutions are shown in fig. 4. For any given lifetime the phase angles increase and the modulations decrease with increasing modulation frequency. The solid lines (top panel) represent the theoretical curves calculated for the lifetimes which yielded minimum value of χ_R^2. Obviously, the calculated values for single-exponential decay accurately reproduce the measured values (○, ●, ▲). The agreement between the measured and calculated data is further illustrated in the lower panel of fig. 4, which shows the deviations between the measured data and the calculated values. The deviations are randomly distributed around zero. This indicates that the single-exponential model is adequate to account for the data, and that the measurements are free of systematic errors. Further evidence for the lack of significant systematic errors is shown below (table 4), in which more complex decays were resolved. The average devia-

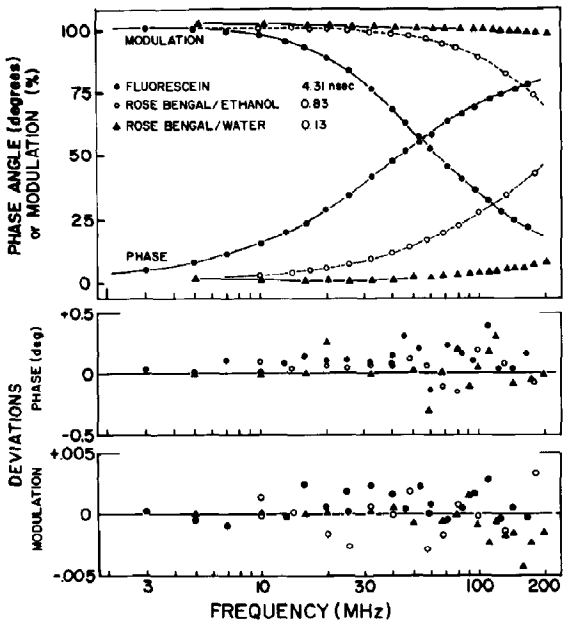

Fig. 4. Phase and modulation data for single-component solutions. Data are shown for fluorescein in water (0.02 M Tris, pH 8) (●), rose bengal in ethanol (○) and in water (▲). See table 2 for additional details. The lower panel shows the deviations between the measured and calculated values.

tions are near 0.2° for phase and 0.002 for modulation. We found these values, or smaller, to be the apparent level of random error for most of our measurements. These values were used for the calculation of χ^2_R.

The measured lifetimes for these fluorophores are summarized in table 2. These values are in precise agreement with earlier time-domain measurements on these same compounds [40,41]. The values of χ^2_R are somewhat less than the expected value near unity. In contrast to photon-counting data [3,4,42], the random errors in phase and modulation cannot be estimated on the basis of counting statistics. Rather, we estimate the level of random error by comparison of the data with the calculated values for cases in which the assumed decay law is appropriate (see refs. 21 and 25). The fact that χ^2_R values are typically less than unity indicates that the actual level of random error is less than 0.2° of phase and less than 0.002 in modulation.

We attempted to fit the data for fluorescein and rose bengal to a double-exponential decay of intensity (table 2). The values of χ^2_R did not substantially decrease, and the amplitude of the assumed second component was negligible. Alternatively, in the case of fluorescein, the lifetime of the assumed second component was similar to the main lifetime, and the value of the second lifetime was highly uncertain. Such results demonstrate that inclusion of an additional component is not justified from the data. These results illustrate the precision and accuracy of our measurements. The degree of random error is small ($\sigma_\phi < 0.2°$ and $\sigma_m < 0.002$), and there do not appear to be any significant systematic errors. We note that these measurements were performed without the use of

Table 2

Measured lifetimes of single-component solutions

All measurements were performed vs. scattered light. Excitation wavelength 442 nm, 25°C. For calculation of χ^2_R we used $\sigma_\phi = 0.2°$ and $\sigma_m = 0.002$. The values in brackets are the estimated uncertainties in the measured lifetimes.

Sample	τ_1 (ns)	τ_2 (ns)	α_2	χ^2_R
Rose bengal/	0.13 (±0.01)	–	–	0.73
water [a]	0.12 (±0.02)	0.40 (±0.81)	0.001	0.57
Rose bengal/	0.83 (±0.01)	–	–	0.50
ethanol [b]	0.83 (±0.01)	0.18 (±2.0)	−0.002	0.54
Fluorescein/	4.31 (±0.02)	–	–	0.56
water [c]	4.22 (±0.18)	3.26 (±1.7)	−0.11	0.38

[a] 0.02 M Tris (pH 8); emission filter, Corning 3-71.
[b] Emission filter, Corning 3-72.
[c] 0.02 M Tris (pH 8); emission filter, Corning 3-72.

standard fluorophores [27], indicating the absence of significant color or geometric artifacts in the PMT time response.

4.2. Two-component mixtures

To illustrate the resolution obtainable from the frequency-domain measurements we examined several two-component mixtures. Our results demonstrate that lifetimes differing by 50% are reliably determined by a single series of measurements. Additionally, by using several data sets obtained for samples in which the proportions of the components are varied, it was possible to resolve lifetimes of 4.1 and 4.5 ns, i.e., a difference of only 10%.

Phase and modulation data for a mixture of anthracene and 9,10-diphenylanthracene are shown in the upper panel fig. 5. Obviously, a good fit to the measured data (●) is provided by an assumed two-component decay law (——). The lower panels show the deviations between the measured and calculated values for the best fit obtainable using a single (O------O) and double (●——●) exponential decay law. For this mixture, in which the decay times differ by only 50%, the experimental deviations found using a single decay time are about 7-fold larger than the random error level of the measurements (fig. 4). For the single-component fit the deviations vary systematically with frequency, indicating that the deviations are not due to random error and are probably due to an inappropriate decay law [25]. Additionally, the value of $\chi^2_R = 12.7$ is clearly unacceptable. The inclusion of a second component in the decay law results in a 45-fold decrease in χ^2_R to 0.28, and the deviations become small and randomly distributed around zero. Once again, the value of χ^2_R indicates that our actual errors in phase and modulation are less than 0.2° and 0.002, respectively. Significantly, the calculated decay times and fractional intensities (4.06 and 6.30 ns, 0.43 and 0.57) are in good agreement with the expected values of 4.08 and 6.31 ns, and $f_1 = f_2 = 0.5$.

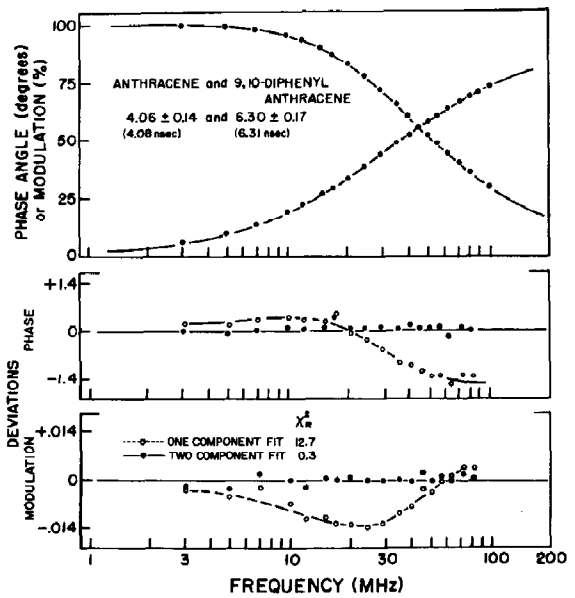

Fig. 5. Phase and modulation data for a two-component mixture of anthracene and 9,10-diphenylanthracene. The lifetime values for anthracene and 9,10-diphenylanthracene are 4.08 and 6.31 ns, respectively, as measured for pure solutions of each compound. The fitting algorithm yielded $f_1 = 0.43$ and $f_2 = 0.57$, in good agreement with the expected values of $f_1 = f_2 = 0.5$. The excitation wavelength was 325 nm, emission filter 0-52, 25°C in ethanol, equilibrated with air.

To illustrate further the resolution obtainable from the frequency-domain measurements we attempted to resolved a mixture of anthracene and 9-methylanthracene. In this case the lifetimes are 4.08 and 4.47 ns, respectively, and thus differ by only 10%. We were not able to determine reliably the lifetimes and fractional intensities using data from a single sample. Instead, we examined four mixtures in which the fractional intensity of anthracene increased from 0.2 to 0.8 (table 3). This procedure is comparable to the 'Global' method described previously [43], except that we varied the fractional intensities by using different proportions of anthracene and 9-methylanthracene, instead of measuring a single sample at several emission wavelengths. This procedure does not yield the emission spectrum of each species, but it is not subject to the restriction that the emission spectra of the components be distinct.

The results of the one- and two-component analysis are shown in table 3. The single-component fit yields an unacceptable value of $\chi^2_R = 6.7$. Inclusion of a second component results in a 25-fold decrease in χ^2_R to 0.27. The recovered life-

Table 3

Analysis of a two-component mixture of anthracene and 9-methylanthracene

Lifetimes	Expected	Observed
Anthracene	4.08	4.13 (0.08) [a]
9-Methylanthracene	4.47	4.41 (0.06)
Fractional intensities of anthracene [b]	0.8	0.86
	0.6	0.45
	0.4	0.24
	0.2	0.05

[a] The value of χ^2_R was 0.27. For a one-component fit $\chi^2_R = 6.7$. $\sigma_\phi = 0.2°$ and $\sigma_m = 0.002$. The values in brackets are the estimated uncertainties.
[b] $f_1 + f_2 = 1.0$.

times (4.13 and 4.41 ns) agree with those expected for anthracene and 9-methylanthracene, 4.08 and 4.47 ns, respectively. The fractional intensities recovered from the fitting algorithm are in reasonable but not consistent agreement with the expected values. However, given the closeness of the two decay times, even this level of agreement must be regarded as satisfactory. From these results it is apparent that frequency-domain fluorometry provides substantial resolution of closely spaced double-exponential decays.

4.3. *Fluorescence decay of NADH*

NADH is often used to test the performance of lifetime instruments because of its short decay time near 0.4 ns [14,27,44]. It has been generally assumed that the decay of NADH was a single exponential. Recently, the decay of NADH was analyzed in detail using a pulse instrument based on a mode-locked argon-ion laser [9]. These workers reported that at 20°C the decay of NADH was doubly exponential with decay times of 0.25 and 0.82 ns, $\alpha_1 = 0.82$ and $\alpha_2 = 0.18$. We measured the frequency-dependent phase and modulation values of NADH at 25°C (fig. 6). Our results are in precise agreement with those of Visser and Hoek [9]. The measurements could not be explained by a single-exponential decay law ($\chi^2_R = 116$). Fitting with a double exponential yielded $\chi^2_R = 2.1$, and lifetimes of 0.20 and 0.86 ns, $\alpha_1 = 0.85$ and $\alpha_2 = 0.15$. Our measurements confirm

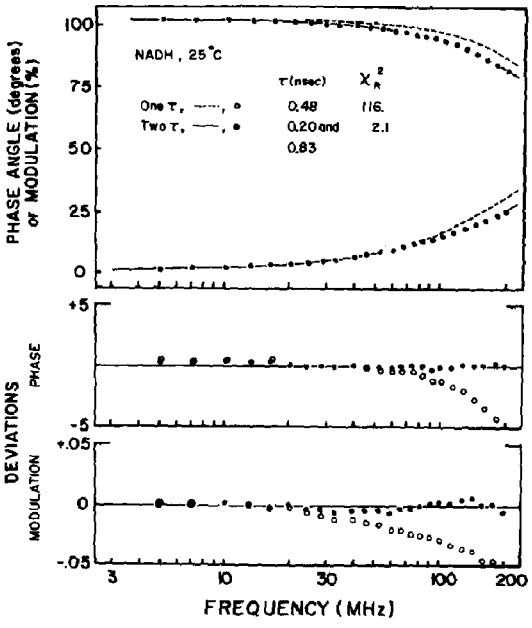

Fig. 6. Fluorescence decay of NADH. NADH was dissolved in 0.02 M Tris (pH 8) 25°C. The excitation wavelength was 325 nm and the emission filter was a Corning 0-52. For the two-component analysis $f_1 = 0.57$ and $f_2 = 0.43$. Similar results were obtained if only the phase data were used in the fitting algorithm.

that the decay of NADH is more complex than a single exponential, and that at least two decay times are required to account for the data. These results demonstrate that the frequency-domain measurements permit resolution of multiexponential decays, even if the decay times are on the subnanosecond time scale.

4.4. *Three-component decays of intensity*

It has been previously noted that the resolution of a three-component decay is considerably more difficult than a two-component decay [42]. Hence it is of interest to test our instrument on a three-component mixture. We examined three-component mixtures of POPOP (1.32 ns), anthracene (4.08 ns) and 9-vinylanthracene (7.73 ns). The resolution of a three-component mixture with a 6-fold range of lifetimes must be regarded as a

difficult problem. We thought it would be necessary to examine a series of samples with different relative concentrations to resolve the decay times. Surprisingly, reliable resolutions were obtained without use of the global method. Fig. 7 shows the two- and three-component fits to a mixture of POPOP, anthracene and 9-vinylanthracene. The two-component fit is easily judged to be unsuccessful because of the systematically varying deviations and the large value of χ^2_R. The two-component fit displays deviations which are about 2-fold larger than the expected level of random error. Inclusion of the third component yields a 10-fold decrease in χ^2_R and more random deviations.

To determine whether such three-component solutions could be reliably analyzed we examined three mixtures with varying proportions of the fluorophores (table 4). In each case χ^2_R decreased 3–10-fold upon incrementation from a two-component to a three-component decay law. Significantly, the recovered decay times and intensities agree with the expected values. For the minor components, such as 9-vinylanthracene is the 5 : 3 : 2 mixture (20% of 9-vinylanthracene), the values are somewhat uncertain. Nonetheless, the frequency-domain measurements yielded consistently satisfactory results for these rather difficult three-component mixtures.

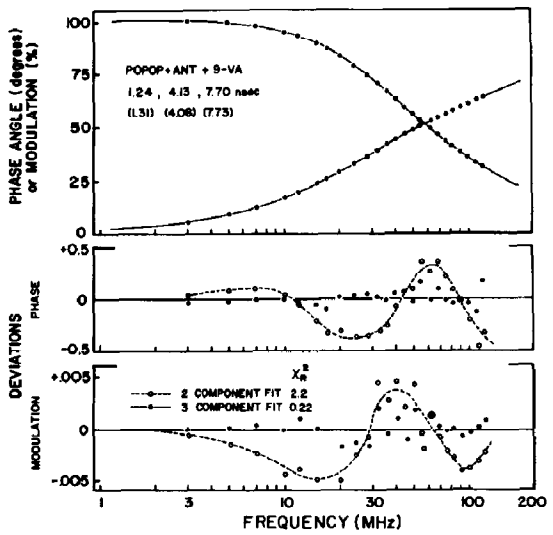

Fig. 7. Analysis of three-component mixture of POPOP, anthracene and 9-vinylanthracene. The measured lifetimes for the individual compounds are shown in brackets. The calculated values of the fractional intensities were 0.15, 0.51 and 0.34 for POPOP, anthracene and 9-vinylanthracene, respectively. The expected values were 0.2, 0.5 and 0.3, respectively.

We also questioned whether analysis of the three-component data with four components would yield any further decrease in χ^2_R. The data set shown in fig. 7 was analyzed repeatedly with different values of the starting parameters. We found no decrease in χ^2_R upon use of a four-component decay law (table 4). In each analysis only three decay times could be recovered. Typically, two of the four decay times were identical. Alternatively, the four decay times were different but the uncertainties in the four decay times were as large as the decay times themselves. This inability of fitting a fourth component to a three-component decay indicates considerable reliability in the resolution of complex decay laws, and also indicates the lack of substantial systematic errors in the measurements. And finally we simultaneously analyzed the data from all three samples (eq. 9). This procedure greatly enhanced the distinction between the two- and three-component fits (table 4). In this case χ^2_R decreased 43-fold when the third decay time was included. This result indicates that, if needed, even more closely spaced three-component decays could be resolved from using frequency-domain fluorometry.

4.5. Measurement of short rotational correlation times

Frequency-domain measurements were used to determine the correlation times of POPOP in fluid solvents. We measured the phase angle difference (Δ_ω) between the perpendicular ($\phi_\perp$) and parallel ($\phi_\parallel$) components of the emission ($\Delta_\omega = \phi_\perp - \phi_\parallel$). Representative data are shown in fig. 8. The differential polarized phase angle (Δ_ω) is dependent upon the rotational rate. For a single correlation time a plot of Δ_ω vs. log ω is nearly Lorentzian in shape. This is not evident in fig. 8 because the rotational rate of POPOP is fast in these solvents, and the maximum value of Δ_ω is displaced beyond our maximum frequency of 200 MHz. The solid

Table 4

Analysis of three-component mixtures of POPOP, anthracene and 9-vinylanthracene

The results are from one series of measurements. Repetition of the measurements yielded essentially identical results. Excitation wavelength, 325 nm; emission filter, Corning 0-52; 25°C.

Intensity values	τ_1 (ns) [a]	τ_2 (ns)	τ_3 (ns)	τ_4 (ns)	f_1	f_2	f_3	f_4	χ^2_R components		
									2	3	4
3/2/5	1.31 (0.04)	4.61 (0.89)	7.69 (0.56)		0.25	0.28	0.47		1.10	0.44	
5/3/2	1.25 (0.03)	4.36 (0.36)	8.87 (1.1)		0.40	0.44	0.15		2.27	0.63	
2/5/3	1.24 (0.05)	4.13 (0.23)	7.70 (0.36)		0.15	0.52	0.34		2.35	0.22	
2/5/3 [b]	1.24 (0.05)	4.13 (0.25)	7.69 (3.1)	7.71 (3.6)	0.15	0.51	0.18	0.16	–	–	0.23
2/5/3 [b]	1.24 (0.07)	4.13 (0.25)	7.85 (1.6)	7.53 (2.3)	0.15	0.51	0.18	0.16	–	–	0.23
2/5/3 [b]	1.23 (0.10)	3.95 (3.8)	5.76 (3.5)	8.09 (8.9)	0.15	0.42	0.18	0.24	–	–	0.23
Global analysis											
3/2/5	1.27 (0.01)	4.18 (0.08)	7.58 (0.10)		0.24	0.25	0.51		23.7	0.55	
5/3/2					0.41	0.36	0.23				
2/5/3					0.16	0.50	0.34				

[a] The measured lifetimes for solution of POPOP, anthracene or 9-vinylanthracene were 1.32, 4.08 and 7.73 ns, respectively. The values in brackets are the estimated uncertainties.

[b] These are typical results for a four-component analysis of these data.

lines represent the calculated values of Δ_ω for the correlation times shown on fig. 8. For these rapid rotational rates it is advantageous to keep r_0 fixed in the fitting algorithm. The value of r_0 was determined by measurements in propylene glycol at −65°C. With this constraint one can readily determine correlation times as short as 0.11 and 0.047 ns for POPOP in ethanol and hexane at 45°C, respectively. For such rapid diffusive motions it is difficult to know if the decay of anisotropy is single or double exponential. In our measurements there was no substantial improvement in χ^2_R upon inclusion of an additional correlation time. These results indicate that short correlation times can be easily determined from frequency-domain fluorometry.

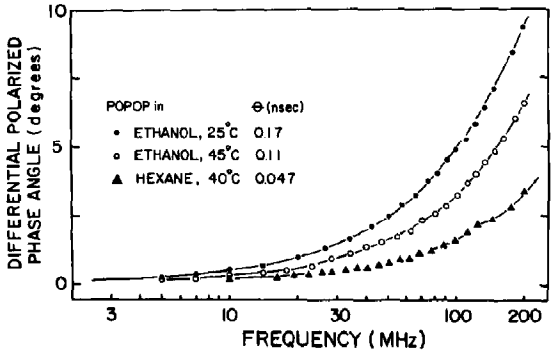

Fig. 8. Differential polarized phase angles for POPOP in fluid solvents. Data are shown for POPOP in ethanol at 25 (●) and 45°C (○), and in hexane of 40°C (▲). Excitation wavelength 325 nm, Corning 0-52 emission filter. Measurements were performed in the T-format configuration [17].

4.6. *Perylene in glycerol, an anisotropic rotator*

It is frequently desirable to resolve multiexponential decays of fluorescence anisotropy. Such complex decays result from segmental motions of protein-bound fluorophores [45], from the asymmetrical shapes of proteins [46] and fluorophores [47,48], and from the anisotropic environments of lipid bilayers [17,49]. We selected perylene because earlier results [47,48] indicated that perylene is an anisotropic rotator, and because this substance could be excited with the more intense 442 nm output of our He-Cd laser. Additionally, because perylene is nonpolar it was likely that its anisotropic motions would persist for excitation on the

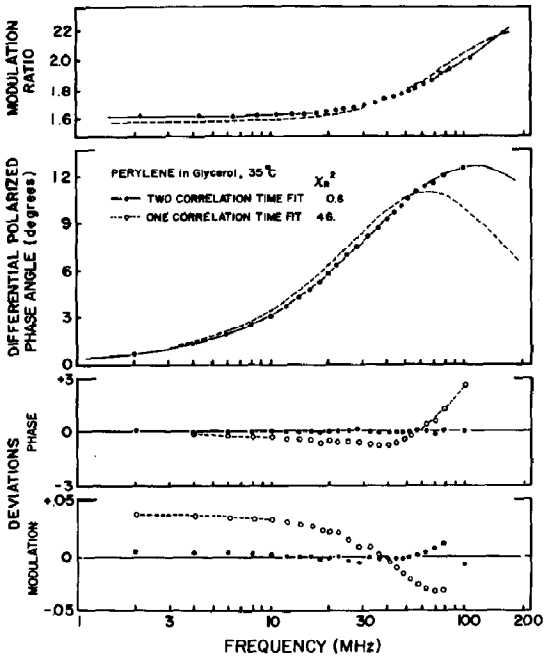

Fig. 9. Differential polarized phase angles and modulation ratios of perylene in glycerol, 35°C.

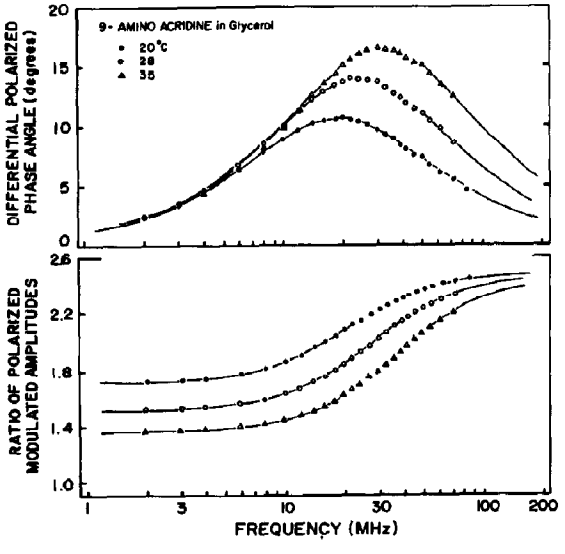

Fig. 10. Differential polarized phase angles and modulation ratios for 9-aminoacridine in glycerol. Excitation wavelength, 442 nm; emission filter, Corning 3-72; T-format.

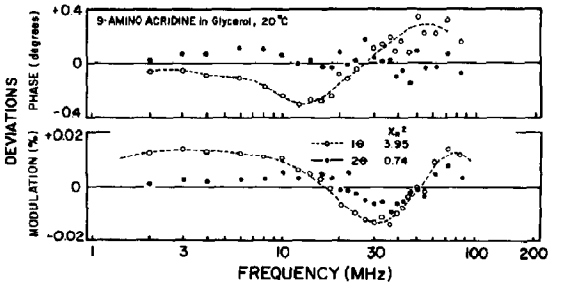

Fig. 11. Deviations between the measured and calculated data for 9-aminoacridine in glycerol, 20°C. Deviations are shown for the fits obtained using one (O------O) and two (●———●) correlation times.

red-edge of its absorption [50,51]. Differential phase and modulation ratio data for perylene are shown in fig. 9. It is evident that these data cannot be fit using a single correlation time (O------O). Inclusion of two correlation times in the fitting algorithm results in a 80-fold decrease in χ^2_R and more random deviations (●———●). The correlation times we observed were 1.5 and 10.8 ns, with $r_0 g_1 = 0.169$ and $r_0 g_2 = 0.184$. These results are in rather good agreement with the time-resolved measurements; these values are 1.7 and 13 ns, with $r_0 g_1 = 0.1$ and $r_0 g_2 = 0.24$ [48].

4.7. 9-Aminoacridine in glycerol, a nearly isotropic rotator

As a final test of our ability to determine complex anisotropy decay laws we examined 9-aminoacridine. According to Mantulin and Weber [47] 9-aminoacridine is an isotropic rotator. More recent results [48] indicated that 9-aminoacridine was nearly isotropic, but in fact it displayed two correlation times with a ratio of 1.4 : 1. We examined 9-aminoacridine in glycerol over a range of temperatures (fig. 10). As the temperature is increased the distribution of Δ_ω is displaced to higher frequencies. These data were analyzed using both the single- and double-correlation time models (table 5). At each temperature rather good fits were obtained using the single-correlation time model. However, there seems little reason to doubt that the double-correlation time model provided a superior fit. In each case the value of χ^2_R decrease

Table 5

Anisotropy decay of 9-aminoacridine in glycerol

Excitation wavelength, 442 nm; emission filter 3-72; T-format. The lifetimes at 20, 28 and 35°C were 15.3, 15.4 and 15.5 ns, respectively.

Temperature (°C)	One-component fit			Two-component fit				
	θ (ns)	r_0	χ^2_R	θ_1	θ_2	$r_0 g_1$	$r_0 g_2$	χ^2_R
20	20.5	0.331 [b]	3.95	12.7	28.7	0.127	0.206	0.74 [a]
28	11.9	0.327	2.80	8.2	14.8	0.121	0.208	0.99
35	7.5	0.323	1.77	5.5	8.9	0.124	0.201	0.91

[a] $\sigma_\phi = 0.1°$ and $\sigma_\omega = 0.005$.
[b] These calculated values are in agreement the value measured at −60°C, which was 0.335.

2–4-fold. Additionally, the deviations became more randomly distributed upon inclusion of the second correlation time (fig. 11). The average ratio of the correlation times is 1.9, in reasonable agreement with the careful studies by Barkley et al. [48]. Our values of $r_0 g_1$ and $r_0 g_2$ are reasonable but not in precise agreement with Barkley et al. [48]. It should be noted that these researchers used additional measurements at different excitation wavelengths to restrain the results. We used measurements at only a single excitation wavelength. Nonetheless, the resolution of such closely spaced correlation times must be regarded as an extremely difficult problem, and this level of agreement is noteworthy.

5. Conclusion

Frequency-domain fluorometry can provide impressive resolution of complex fluorescence decay kinetics, and will thus be widely useful in chemical and biochemical research.

Acknowledgements

This work was supported by grants PCM 82-10878 and 81-20068 from the National Science Foundation.

References

1 R.F. Steiner, Excited states of biopolymers (Plenum Press, New York, 1983).
2 J.R. Lakowicz, Principles of fluorescence spectroscopy (Plenum Press, New York, 1983).
3 J.N. Demas, Excited state lifetime measurements (Academic Press, New York, 1983).
4 M.G. Badea and L. Brand, Methods Enzymol. 61 (1979) 378.
5 R.R. Alfono, Biological events probed by ultrafast laser spectroscopy (Academic Press, New York, 1982).
6 L.T. Libertini and E.W. Small, Rev. Sci. Instrum. 54 (1983) 1458.
7 E.W. Small, L.J. Libertini and I. Isenberg, Rev. Sci. Instrum. 55 (1984) 879.
8 A.V. Hoek, J. Vervoort and A.J.W.G. Visser, J. Biochem. Biophys. Methods 7 (1983) 243.
9 A.J.W.G. Visser and A.V. Hoek, Photochem. Photobiol. 33 (1981) 35.
10 E.Z. Gaviola, Z. Phys. 42 (1927) 852.
11 E.A. Bailey and G.K. Rollefson, J. Chem. Phys. 21 (1953) 1315.
12 J.B. Birks and D.J. Dyson, J. Sci. Instrum. 38 (1961) 282.
13 A. Muller, R. Lumry and H. Kokubun, Rev. Sci. Instrum. 36 (1965) 1214.
14 R.D. Spencer and G. Weber, Ann. N.Y. Acad. Sci. 158 (1969) 361.
15 D.M. Jameson and G. Weber, J. Phys. Chem. 85 (1981) 953.
16 J.R. Lakowicz and H. Cherek, J. Biol. Chem. 256 (1981) 6348.
17 J.R. Lakowicz, F.G. Prendergast and D. Hogen, Biochemistry 18 (1979) 508.
18 E. Gratton and M. Limkeman, Biophys. J. 44 (1983) 315.
19 E.R. Menzel and Z.D. Popovic, Rev. Sci. Instrum. 49 (1978) 34.
20 H.P. Haar and M. Hauser, Rev. Sci. Instrum. 49 (1978) 632.
21 E. Gratton, J.R. Lakowicz, B. Maliwal, H. Cherek, G. Laczko and M. Limkeman, Biophys. J. 46 (1984) 479.
22 J.R. Lakowicz, H. Cherek, B. Maliwal and E. Gratton, Biochemistry (1984) in the press.
23 J.R. Lakowicz, H. Cherek, B.P. Maliwal, G. Laczko and E. Gratton, J. Biol. Chem. 259 (1984) 10967.
24 J.R. Lakowicz, H. Cherek, G. Laczko and E. Gratton, Biochim. Biophys. Acta (1984) in the press.

25 J.R. Lakowicz, E. Gratton, G. Laczko, H. Cherek and M. Limkeman, Biophys. J. 46 (1984) 463.
26 P.R. Bevington, Data reduction and error analysis for the physical sciences (McGraw-Hill, New York, 1969).
27 J.R. Lakowicz and H. Cherek, J. Biochem. Biophys. Methods 5 (1981) 131.
28 E. Gratton and R. Lopez-Delgado, Il Nuovo Cimento 56B (1980) 110.
29 I.P. Kaminov, An introduction to electrooptic devices (Academic Press, New York, 1974).
30 J. Wilson and J.F.B. Hawkes, Optoelectronics, an introduction (Prentice/Hall International, Englewood Cliffs, NJ, 1983).
31 J.M. Bennet and H.E. Bennet, in: Handbook of optics, eds. W.G. Driscoll and W. Vaughan (McGraw-Hill, New York, 1978) ch. 10.
32 Technical literature, lasermetrics, light modulators and Q-switch operations manual.
33 I. Salmeen and L. Rimai, Biophys. J. 20 (1977) 335.
34 W.R. Ware, M. Pratinidki and R.K. Bauer, Rev. Sci. Instrum. 54 (1983) 1148.
35 H.D. Wolpert, Photonics Spectra December (1983) p. 71.
36 S. Kinoshita and T. Kushida, Rev. Sci. Instrum. 53 (1982) 469.
37 S. Kinoshita, H. Ohta and T. Kushida, Rev. Sci. Instrum. 52 (1981) 572.
38 G. Weber, J. Chem. Phys. 66 (1977) 4081.
39 V.V. Solodovnikov, Introduction to the statistical dynamics of automatic control systems (Dover Publication, New York, 1960).
40 H.E. Zimmerman, J.H. Penn and C.W. Carpenter, Proc. Natl. Acad. Sci. U.S.A. 79 (1982) 2128.
41 K.G. Spears, L.E. Cramer and L.D. Hoffland, Rev. Sci. Instrum. 49 (1978) 255.
42 A. Grinvald and I.Z. Steinberg, Anal. Biochem. 59 (1974) 583.
43 J.R. Knutson, J. Beechem and C. Brand, Photochem. Photobiol. 37 (1983) S20.
44 A. Gafni and L. brand, Biochemistry 15 (1976) 3165.
45 I. Munro, I. Pecht and L. Stryer, Proc. Natl. Acad. Sci. U.S.A. 76 (1979) 56.
46 E.W. Small and I. Isenberg, Biopolymers 16 (1977) 1907.
47 W.W. Mantulin and G. Weber, J. Chem. Phys. 66 (1977) 4092.
48 M.D. Barkley, A.A. Kowalczyk and L. Brand, J. Chem. Phys. 75 (1981) 3581.
49 S. Kawato, K. Kinosita and A. Ikegami, Biochemistry 16 (1977) 2319.
50 B. Valeur and G. Weber J. Chem. Phys. 69 (1978) 2393.
51 J.R. Lakowicz, Biophys. Chem. 19 (1984) 13.